Measurement 236 (2024) 115078

Contents lists available at ScienceDirect

Measurement

journal homepage: www.elsevier.com/locate/measurement

Probabilistic impact localization in composites using wavelet scattering transform and multi-output Gaussian process regression

Shivam Ojha [a], Naveen Jangid [a], Amit Shelke [a], Anowarul Habib [b,*]

[a] Department of Civil Engineering, Indian Institute of Technology, Guwahati, 781039, Assam, India
[b] Department of Physics and Technology, UiT The Arctic University of Norway, Tromsø, 9037, Norway

ARTICLE INFO

Keywords:
Acoustic emission
AE source localization
Multi-output Gaussian process regression
Probabilistic machine learning
Structural health monitoring
Wavelet scattering transformation

ABSTRACT

Data-driven machine-learning models offer considerable promise for acoustic source localization. However, many existing models rely on training data that correlates time-of-flight (TOF) measurements with source locations, yet they struggle to handle the complexities arising from nonlinear wave propagation in materials with varying properties. Furthermore, these models overlook the noise and uncertainties inherent in real-world experiments when predicting outputs. This paper aims to bridge a gap in impact localization for such structures, particularly focusing on scenarios involving noisy field measurements. This study proposes a framework based on probabilistic machine learning to identify impact locations, utilizing wavelet scattering transform (WST) and Multi-Output Gaussian Process Regression (moGPR). WST extracts informative features from Lamb waves, capturing relevant signatures for training the probabilistic machine learning model, while moGPR estimates correlated impact location coordinates (x, y) while accounting for inherent uncertainties in the data. To assess the proposed method's performance in handling measurement uncertainties, an experiment was conducted using a CFRP composite panel instrumented with a sparse array of piezoelectric transducers. The results demonstrate that the probabilistic framework effectively addresses measurement uncertainties, enabling reliable source location estimation with confidence intervals and providing valuable insights for decision-making.

1. Introduction

The increasing prevalence of anisotropic plates and shells within aeronautical, automotive, and wind energy applications highlights their value for achieving outstanding stiffness-to-weight ratios. However, alongside this growing popularity, concerns regarding the long-term integrity of these composite structures have emerged. A significant worry is their susceptibility to impact events like hail strikes, bird collisions, and ground support equipment interactions [1,2].

Structural health monitoring (SHM) is vital for condition-based maintenance (CBM), promising reduced life-cycle costs and enhanced aircraft safety. It leverages sparse ultrasonic transducer arrays employing guided ultrasonic waves (GUWs) in both active and passive modes for microscale defect detection and localization [3]. Active mode utilizes acoustic actuators as the energy source, while passive mode relies on impacts as the acoustic emission [4–6]. Sparse sensor arrays that transmit and receive guided ultrasonic waves (GUWs) offer exceptional defect detection capabilities through triangulation in case of isotropic plates [7–9].

The conventional AE source localization involves time-of-flight (TOF) measurements and subsequent calculations using non-linear equations or error minimization [10–15]. However, this approach becomes computationally expensive with increasing sensors. Additionally, TOF accuracy is critical, and minor errors can significantly impact localization. Sources of error include systematic errors, dispersion, noise, and temperature variations. Noise is inherent in experimental setups, and methodological uncertainties can further hamper results. Various approaches can be found in the literature that address the uncertainties. Recently, [16] presented a convex model-based reduced-order model for developing an uncertain Hankel matrix. They also proposed a Delaunay triangulation method for position estimation in complex trajectories [17]. Further, several advanced methods have been developed for incorporating uncertainties into models for system identification, position localization, and automatic control systems [18–21]. Specifically for acoustic source localization, [22] has proposed the probabilistic frameworks based on the Extended Kalman Filter (EKF) and Unscented Kalman Filter (UKF) algorithm to estimate AE source location and wave velocity for isotropic and anisotropic velocity [23,24]. It is easier to evaluate the propagation velocity in isotropic plates and thus the location of damage identified through evaluating time of

* Corresponding author.
E-mail address: anowarul.habib@uit.no (A. Habib).

https://doi.org/10.1016/j.measurement.2024.115078
Received 15 April 2024; Received in revised form 16 May 2024; Accepted 6 June 2024
Available online 14 June 2024

flight observations. However, these techniques struggle in the case of an anisotropic plate, as the wave velocity varies in different directions [15,22]. The discussion highlights that traditional approaches to acoustic emission (AE) source localization primarily rely on time-domain analyses and basic signal processing techniques. These approaches provide a foundation, but they can struggle to handle the complexities arising from non-linear wave propagation in materials with varying properties like anisotropic or heterogeneous materials. As a result, developing a source localization approach that works effectively in real-world structures remains a challenge. Several studies have proposed strategies to improve AE source location accuracy, particularly for structures with simple geometries in laboratory settings. These strategies include methods based on wave velocity [25,26], methods that do not rely on wave velocity [27–31], statistical methods [32,33], and mapping techniques [34,35].

Recent advancements in data-driven machine learning methods offer new avenues for AE source localization through Lamb wave characterization. The data-driven regression models based on relevant parameters are gaining traction for AE source identification [36–38]. One prominent approach is the Bayesian framework based on Gaussian Process (GP) regression, which has been applied for AE source localization in complex structures [39]. Similarly, [40] explored Bayesian methods and heteroscedastic Gaussian processes for improved source localization [41]. During the training, machine learning models learn the inherent system's characteristics by mapping input data to desired outputs. These training data for most of the models used in the past involve time of flight measurements or statistical properties of acoustic signals like, rise time, counts, average signal levels, and more. However, limited research is available that leverages the Lamb wave signatures and ML models to achieve the desired output. This paper introduces wavelet scattering transform (WST) to capture Lamb wave signatures and generate rich feature sets for the machine learning model [42,43]. WST offers several advantages: (1) It provides resolutions in both time and frequency domains, making it robust to signal variations. (2) WST features remain stable even with signal deformations, ensuring reliable analysis. (3) It retains high-frequency information crucial for classification tasks.

Furthermore, [44] identified three key properties desired for feature extraction in machine learning models: multiscale representation, hierarchical symmetry linearization, and sparse representation. Notably, WST possesses all these properties, making it well-suited for the proposed AE source localization framework. Despite adopting a robust feature extractor for capturing intrinsic Lamb wave signatures, the source location is two-dimensional and a correlation exists between coordinates. While [30] explored separate models for each source location coordinate using an energy-based approach, deep learning offers an alternative. Multi-layer perceptron (MLP) models can handle correlated outputs, but they have limitations: (1) Large training data requirements, (2) Inability to incorporate uncertainties in data and modeling and (3) Lack of probabilistic source location estimates

This research addresses a gap in impact localization for anisotropic composite structures, particularly when dealing with noisy field measurements. We propose a novel framework utilizing probabilistic machine learning to identify the impact location. This study leverages wavelet scattering transform (WST) to generate a feature matrix that captures relevant Lamb wave signatures for training the machine learning model. Notably, the impact location coordinates (x, y) are inherently correlated. Traditional algorithms like Gaussian Process Regression (GPR) can handle input–output correlations, but they struggle with correlated outputs [45,46]. The proposed framework is compared with the five other approaches present in the literature. Here, the paper employs multi-output Gaussian Process Regression (moGPR) due to its suitability for handling correlated data, such as the relationship between impact location coordinates (x, y) and Lamb wave signatures in anisotropic composites. Compared to conventional and MLP methods, the proposed moGPR framework presents the following advantages:

1. Uncertainty incorporation: moGPR inherent Gaussian structure allows it to incorporate noise and uncertainties present in real-world data.
2. Confidence Intervals: Unlike deterministic methods, moGPR provides confidence intervals for estimated impact locations, aiding decision-making processes.
3. Data Efficiency: moGPR requires sparse data for training compared to AI methods like multi-layer perceptron methods which are data-hungry. Further, it avoids issues like vanishing or exploding gradients, making it well-suited for scenarios with limited data.

Overall, this framework offers a robust, reliable, and efficient solution for impact localization within the Structural Health Monitoring (SHM) framework for anisotropic composite structures, especially in the presence of noisy data.

2. Methodology

This work introduces a novel, automated probabilistic framework for impact localization in anisotropic composites. The framework leverages wavelet scattering transform (WST) and multi-output Gaussian process regression (moGPR) to account for measurement and process uncertainties inherent in experiments [47]. WST extracts informative features from Lamb waves, enabling moGPR to map these signatures to the estimated impact location. The proposed framework is applied to a carbon fiber-reinforced polymer (CFRP) composite panel instrumented with a sparse array of piezoelectric transducers. The details of the methodology are discussed below:

2.1. Wavelet scattering transformation

The wavelet scattering transform reconstructs the signal which are translation invariant, stable, and informative. Its robustness to deformations and ability to preserve class discriminability make it preferable for the feature extraction of Lamb wave signatures. Notably, prior studies [48–51] have showcased its exceptional practical performance in classification contexts. In line with the conventions established by [51], let us denote the signal under analysis as $f(t)$. Here, the low-pass filter ϕ and wavelet function ψ are tailored to construct filters encompassing the signal frequencies. Specifically, $\phi_J(t)$ represents the low-pass filter facilitating local translation-invariant descriptions of f at a predefined scale T, while Λ_k denotes the wavelet index family with octave frequency resolution Q_k. Through dilation of the wavelet ψ, the multiscale high-pass filter banks $\left\{\psi_{j_k}\right\}_{j_k \epsilon \Lambda_k}$ are constructed.

In this research, a wavelet scattering transform is deployed, which undergoes iterations involving traditional wavelet transforms, nonlinear modulus operations, and averaging operators. The initial convolution $S_0 f(t) = f \times \phi_J(t)$ produces a local translation-invariant feature of f, yet it leads to the loss of high-frequency information. To address this, a wavelet modulus transform, outlined in Eq. (1), is employed to recover the lost high frequencies.

$$|W_1|f = \{S_0 f(t), |f \times \psi_{j_1}(t)|\}_{j_1 \epsilon \Lambda_1} \tag{1}$$

The first-order and second-order scattering coefficients are obtained by averaging the wavelet modulus coefficients with ϕ_J

$$\begin{aligned} S_1 f(t) &= \{|f \times \psi_{j_1}| \times \phi_J(t)\}_{j_1 \epsilon \Lambda_1} \\ S_2 f(t) &= \{||f \times \psi_{j_1}| \times \psi_{j_2}| \times \phi_J(t)\}_{j_i \epsilon \Lambda_i}, i = 1, 2. \end{aligned} \tag{2}$$

To recover the information lost by averaging, noting that $S_1 f(t)$ can be seen as the low-frequency component of $|f \times \phi_{(j_1)}|$, we can extract complementary high-frequency coefficients by Eq. (3)

$$|W_2||f \times \psi_{j_1}| = \{S_1 f(t), ||f \times \psi_{j_1}| \times \psi_{j_2}(t)|\}_{j_2 \epsilon \Lambda_2} \tag{3}$$

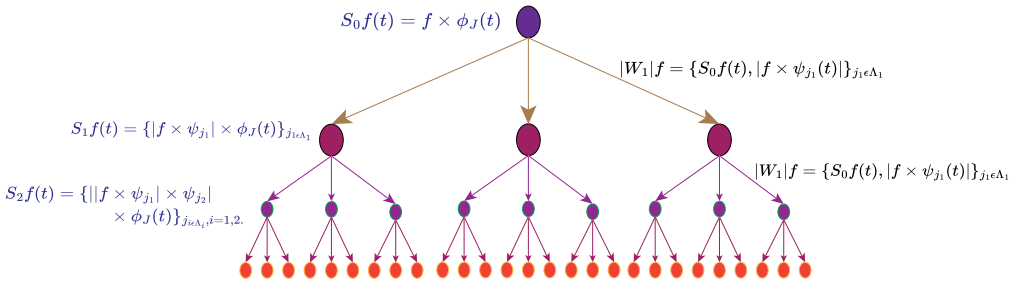

Fig. 1. A wavelet scattering network in the tree mode.

Thus, by iterating the process, we obtain

$$U_m f(t) = \{|||f \times \psi_{j_1}| \times \cdots | \times \psi_{j_m}|\}_{j_i \epsilon \Lambda_i}, i = 1, 2, \ldots, m. \tag{4}$$

Averaging $U_m f(t)$ with ϕ_J gives the mth $-$ *order* scattering coefficients

$$S_m f(t) = \{|||f \times \phi_{j_1}| \times \cdots | \times \phi_{j_m}| \times \phi_J(t)\}_{j_i \epsilon \Lambda_i}, i = 1, 2, \ldots, m. \tag{5}$$

This scattering process in the tree mode is illustrated in Fig. 1. The final scattering matrix is given as

$$Sf(t) = \{S_m f(t)\}_{0 \le m \le l} \tag{6}$$

This aggregates scattering coefficients of all orders to describe the features of an input signal, where l is the maximal decomposition order.

The network achieves translation invariance up to a tunable scale, thanks to the averaging effect of the low-pass filter ϕ_J. Additionally, the features, $Sf(t)$, inherit stability to local deformations from the wavelet transform. This makes scattering decomposition ideal for capturing subtle changes in Lamb wave signals which are crucial for damage assessment in anisotropic composite panels but difficult to measure directly. Therefore, this study leverages a wavelet scattering network to generate robust representations of Lamb wave signatures. Furthermore, it can be shown that the energy in scattering coefficients rapidly diminishes with increasing layer depth, with nearly 99% concentrated in the first two layers [49,51]. To exploit this property and significantly reduce computational complexity, we employed a second order scattering network for Lamb wave feature extraction.

2.2. Gaussian process regression

In Gaussian process regression, observations are characterized using optimized mean functions and covariance, or kernel functions [52]. Typically, for many tasks, the mean function is set to zero, and observations are trained solely using the kernel function. Let the dataset be modeled as $f(\mathbf{x}) \sim GP(m(\mathbf{x}), \kappa(\mathbf{x}, \mathbf{x}'))$, where $m(x) = \mathbf{E}[f(\mathbf{x})]$ denotes the mean function, and $\kappa(\mathbf{x}, \mathbf{x}') = \mathbf{E}\left[(f(\mathbf{x}) - m(\mathbf{x}))(f(\mathbf{x}') - m(\mathbf{x}'))^T\right]$ represents the kernel or covariance function. Consequently, for a finite set of observations, this process is jointly Gaussian, given by:

$$p(\mathbf{f}|\mathbf{X}) = \mathcal{N}(\mathbf{f}|\mu, \mathbf{K}) \tag{7}$$

where $K_{ij} = \kappa(\mathbf{x}_i, \mathbf{x}_j)$ and $\mu = (m(\mathbf{x}_1), \ldots, m(\mathbf{x}_N))$. Consider a training dataset $\mathcal{D} = \{(\mathbf{x}_i, f_i), i = 1 : N\}$, where $f_i = f(\mathbf{x}_i)$ denotes the noise-free observation of the function evaluated at $\mathbf{x}_i$. Given a test set $\mathbf{X}*$ of size $N* \times D$, the objective is to predict the function outputs $\mathbf{f}*$. As per the definition of the Gaussian process, the joint distribution follows the specified form.

$$\begin{pmatrix} \mathbf{f} \\ \mathbf{f}_* \end{pmatrix} \sim \mathcal{N}\left(\begin{pmatrix} \mu \\ \mu_* \end{pmatrix}, \begin{pmatrix} \mathbf{K} & \mathbf{K}_* \\ \mathbf{K}_*^T & \mathbf{K}_{**} \end{pmatrix}\right) \tag{8}$$

where $\mathbf{K} = \kappa(\mathbf{X}, \mathbf{X})$ is $N \times N, \mathbf{K}_* = \kappa(\mathbf{X}, \mathbf{X}_*)$ is $N \times N_*$, and $\mathbf{K}_{**} = \kappa(\mathbf{X}_*, \mathbf{X}_*)$ is $N_* \times N_*$. Using Bayesian transformation, the posterior can be written as

$$\begin{aligned} p(\mathbf{f}_* \mid \mathbf{X}_*, \mathbf{X}, \mathbf{f}) &= \mathcal{N}(\mathbf{f}_* \mid \mu_*, \mathbf{\Sigma}_*) \\ \mu_* &= \mu(\mathbf{X}_*) + \mathbf{K}_*^T \mathbf{K}^{-1}(\mathbf{f} - \mu(\mathbf{X})) \\ \mathbf{\Sigma}_* &= \mathbf{K}_{**} - \mathbf{K}_*^T \mathbf{K}^{-1} \mathbf{K}_* \end{aligned} \tag{9}$$

In scenarios involving noisy observations, the covariance matrix $\mathbf{K}$ is adjusted incorporating the noise variance σ_y^2 by adding it to the diagonal elements, resulting in $\mathbf{K} + \sigma_y^2 \mathbf{I} N \triangleq \mathbf{K}\text{mod}$. The squared exponential kernel is defined as:

$$k(x_1, x_2) = \sigma^2 \exp\left(-\frac{\|x_1 - x_2\|^2}{2l^2}\right) \tag{10}$$

where, $l > 0$ and $\sigma^2 > 0$ are the length scale and variance parameters.

With its robust capabilities, Gaussian Process Regression (GPR) stands out as a powerful probabilistic machine learning tool adept at capturing inherent uncertainties and offering probabilistic estimates. This makes it highly suitable for impact localization tasks. However, it is worth noting that GPR is limited in its ability to provide multiple outputs, such as simultaneous x and y coordinates, and tends to overlook correlations between these outputs. To address the shortcomings, this paper proposes a probabilistic framework based on the multi-output Gaussian process regression (moGPR) for impact localization. The detailed mathematics of the moGPR is illustrated in the next section.

2.3. Multi-output Gaussian process regression

The GPR model for observations with noise in a single-output scenario is described by $y(x_i) = f(x_i) + \epsilon_i$, where $f(x) \sim GP(0, k(x, x'))$ and the noise $\epsilon_i \sim \mathcal{N}(0, \sigma^2)$. Given a training set $D = \{(x_i, y(x_i)) | i = 1, 2, \ldots, N\}$, the joint distribution of these noisy observations can be formulated as follows:

$$\begin{bmatrix} y(\mathbf{x}_1) \\ \vdots \\ y(\mathbf{x}_N) \end{bmatrix} \sim \mathcal{N}\left(\begin{bmatrix} 0 \\ \vdots \\ 0 \end{bmatrix}, \begin{bmatrix} k(\mathbf{x}_1, \mathbf{x}_1) & \cdots & k(\mathbf{x}_1, \mathbf{x}_N) \\ \vdots & \ddots & \vdots \\ k(\mathbf{x}_N, \mathbf{x}_1) & \cdots & k(\mathbf{x}_N, \mathbf{x}_N) \end{bmatrix} + \sigma^2 \begin{bmatrix} 1 & \cdots & 0 \\ \vdots & \ddots & \vdots \\ 0 & \cdots & 1 \end{bmatrix}\right) \tag{11}$$

The hyperparameters of the kernel function are optimized through Bayesian optimization, and the prediction can be made through calculating the posterior $p(f(\mathbf{x}_*) \mid \mathbf{y})$. Here, it should be noted that there is only a single dimension of the output (y) predicted using a single kernel function (κ). Let us suppose that for the same input parameters, (x_i) and the observations have two dimensions that are correlated. Thus, the observations are modeled using $y_1(x_i) = f_1(x_i) + \epsilon_i$ and $y_2(x_i) = f_2(x_i) + \epsilon_i$. The training dataset will now be represented as $D_1 = \{(x_i, y_1(x_i)) \mid i = 1, 2, \ldots, N\}$ and $D_2 = \{(x_i, y_2(x_i)) \mid i = 1, 2, \ldots, N\}$, where the joint distribution is given by $y_1\ N(0, k_1 + \sigma_1^2 I)$ and $y_2\ N(0, k_2 + \sigma_2^2 I)$ respectively. It can be written combined as follows:

$$\begin{bmatrix} y_1 \\ y_2 \end{bmatrix} \sim \mathcal{N}\left(\begin{bmatrix} 0 \\ 0 \end{bmatrix}, \begin{bmatrix} k_1 & cov(f_1(x_i) \cdot f_2(x_i)) \\ cov(f_1(x_i) \cdot f_2(x_i)) & k_2 \end{bmatrix}\right)$$

$$+\begin{bmatrix}\sigma_1^2 I & 0\\ 0 & \sigma_2^2 I\end{bmatrix}\Bigg) \tag{12}$$

The cross terms of the kernel matrix are difficult to calculate and depend on the different configurations of inputs and the correlation of outputs. These covariance functions that relate to the correlation in the output domain are evaluated through the concept of interdomain Gaussian process and coregionalization [53]. In the current work, the outputs are considered as the interrelated elements of the constitutive matrix. Therefore, these quantities rely on a transformation of $f(\cdot)$ to a different domain giving rise to the interdomain Gaussian process. Once again, multi-output function is denoted by $f_p(\mathbf{x})$ which is the pth output of $f(\cdot)$ at the input $\mathbf{x}$. A prior over such functions is a multioutput Gaussian process [54] when the distribution of a vector of values is

$$\mathbf{f} = \left\{ f_{p_n}(\mathbf{x}_n) \right\}_{n=1}^{N},\ \mathbf{f} \in \mathbb{R}^N \tag{13}$$

is Gaussian distributed. Here, $\mathbf{x}_n$ is the input and the corresponding output p_n. The kernels for the multioutput Gaussian process on the input space $\mathcal{X}$ is written as:

$$k : \mathcal{X} \times \mathcal{X} \to \mathbb{R},\ k(\mathbf{x}, \mathbf{x}') = \mathbb{C}_{f(\cdot)}\left[f(\mathbf{x}), f(\mathbf{x}') \right], \tag{14}$$

where a covariance matrix for all outputs is returned [55,56]. In an alternative approach that is used in this paper, the index of the multiple output is treated as another input. In other words, multioutput kernels are functions on the input space $\mathcal{X}$ extended by the index of the output, represented as follows:

$$k : (\mathcal{X}, \mathbb{N}) \times (\mathcal{X}, \mathbb{N}) \to \mathbb{R},\ \mathbb{C}_{f(\cdot)}\left[f_p(\mathbf{x}), f_{p'}(\mathbf{x}') \right] = \mathbb{E}_{f(\cdot)}\left[f_p(\mathbf{x}) f_{p'}(\mathbf{x}') \right]$$
$$= k\left(\mathbf{x}, p, \{\mathbf{x}', p'\}\right) \tag{15}$$

Now, it is also important to discuss priors on the correlations between multiple outputs [54]. The approach used in this paper is linear model of coregionalization [57]. The multi-output function $f(\cdot)$ from a linear transformation $W \in \mathbb{R}^{P \times L}$ of L independent functions $g_\ell(\cdot)$ as:

$$\begin{aligned} g_\ell(\cdot) &\sim \mathcal{GP}\left(0, k_\ell(\cdot, \cdot')\right)\\ g(\mathbf{x}) &= \left\{ g_\ell(\mathbf{x}) \right\}_{\ell=1}^{L}\\ f(\mathbf{x}) &= W g(\mathbf{x}) \end{aligned} \tag{16}$$

with $f(\mathbf{x}) \in \mathbb{R}^P$ and $g(\mathbf{x}) \in \mathbb{R}^L$. Thus, the covariance is rewritten as the

$$k\left(\mathbf{x}, p, \{\mathbf{x}', p'\}\right) = \mathbb{E}_g\left[\left[W g(\mathbf{x}) g(\mathbf{x}')^\top W^\top \right]_{pp'} \right] = \sum_{\ell=1}^{L} W_{p\ell} k_\ell(\mathbf{x}, \mathbf{x}') W_{p'\ell} \tag{17}$$

To effectively handle correlated outputs and uncertainties, the research framework employs moGPR as a robust probabilistic machine learning solution for mapping Lamb wave signatures to acoustic source locations.

3. Experimental study

The proposed probabilistic framework is validated through an experiment on carbon-fiber-reinforced polymer (CFRP) composites as shown in Fig. 2(a). This research utilizes an anisotropic CFRP composite panel, with a nominal thickness of 2 mm and dimensions of 600 mm by 600 mm. To simulate the impacts, a Teflon sphere with a diameter of 13.4 mm and weight of 10 g is employed, dropped from a height of 0.3 m onto the panel to generate acoustic waves. These waves are then captured by five strategically placed piezoelectric sensors labeled S1 through S5, positioned based on specific coordinates to optimize the detection of acoustic emissions generated from the impacts. Considering the origin in the bottom left corner of the square composite, the location of piezoelectric sensors on the composite panel is highlighted in Table 1. Here, Teflon sphere is used because of its low impedance value that results in reduced reverberations providing a cleaner and more easily analyzable acoustic emission signal. Additionally, Teflon's softer nature makes it a safer choice for non-destructive testing of composite materials.

Table 1
Details of the location of piezoelectric sensors on composite panel.

Sensor	X ordinate (mm)	Y ordinate (mm)
S1	75	75
S2	305	75
S3	535	75
S4	19	535
S5	42	535

The procedure begins with the calibration and setup of the sensors on the panel, ensuring their placement adheres to the specified coordinates for optimal spatial coverage. Impacts are then generated at various points on the panel, specifically at intersecting nodes created by grid lines as illustrated in schematic diagrams as shown in Fig. 2(b). This methodical approach to generating impacts across the panel ensures a rich dataset of varying impact locations, critical for the training and validation of the moGPR algorithm. The acoustic emissions recorded by the sensors form the primary dataset, which is subsequently processed using wavelet scattering transform. By splitting the dataset into training and testing subsets with a ratio of 80:20, the experimental setup facilitated the development and optimization of the proposed probabilistic machine learning framework while enabling a thorough assessment of their accuracy and reliability in localizing damage in anisotropic plates based on acoustic emission signals. The details of the proposed framework are illustrated in the next section.

4. Proposed algorithm

This work proposes a unified framework for feature extraction and modeling leveraging the wavelet scattering transform and multi-output Gaussian process regression. The framework is stochastic and is designed particularly to handle sparse data perturbed by noise and uncertainty in the observations. The earlier methods in acoustic source localization have predominantly focused on a time of flight observations and do not directly analyze the waveform captured by sensors for feature extraction. These methods are foundational, however lack in handling the intricate nature of acoustic responses, especially in complex materials or under variable environmental conditions. Further, the traditional approaches use single-output prediction models, which neglect the correlation between the output variables, leading to less accurate localization. Thus, this algorithm employs wavelet scattering transform, which extracts robust and discriminating features that are inherently more capable of capturing the subtle anomaly and nonlinear characteristics of these signals compared to traditional methods. Moreover, the moGPR is introduced to consider model multiple outputs corresponding to the spatial coordinates of acoustic source locations and the correlation between output parameters as well as the uncertainties in the input parameters. Thus, uncertainties are incorporated that help in the estimation of output distribution instead of a point estimate leading to uncertainty quantification as well. The primary steps for the proposed algorithm are listed below and are graphically represented in Fig. 3.

Step 1 - Pre-processing. The algorithm begins with the pre-processing of raw sensor data. This stage involves filtering to remove noise and irrelevant frequencies. Further, normalization is then applied to ensure uniformity in signal amplitude across all sensors, which is crucial for the subsequent feature extraction and modeling phases.

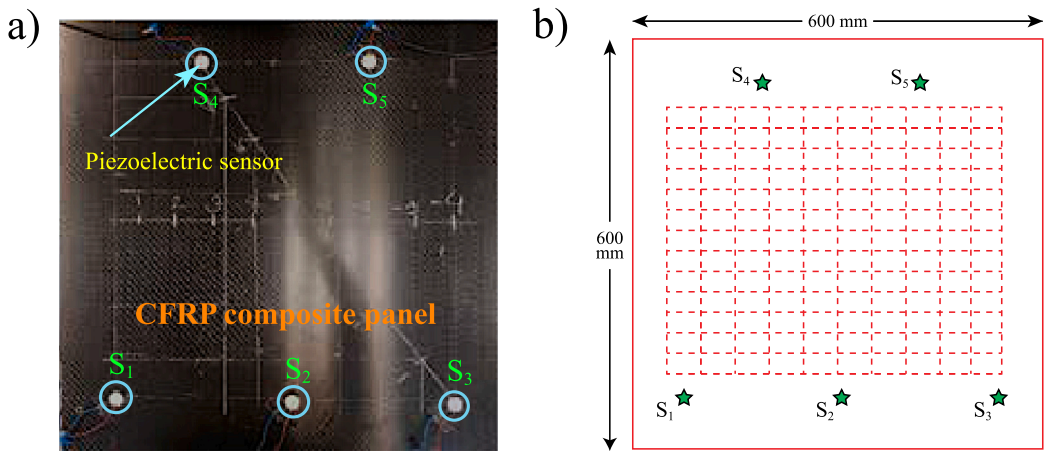

Fig. 2. The experiment is conducted on the composite panel with mounted piezoelectric sensors as shown in (a) and the impact locations are the grid points as provided in (b).

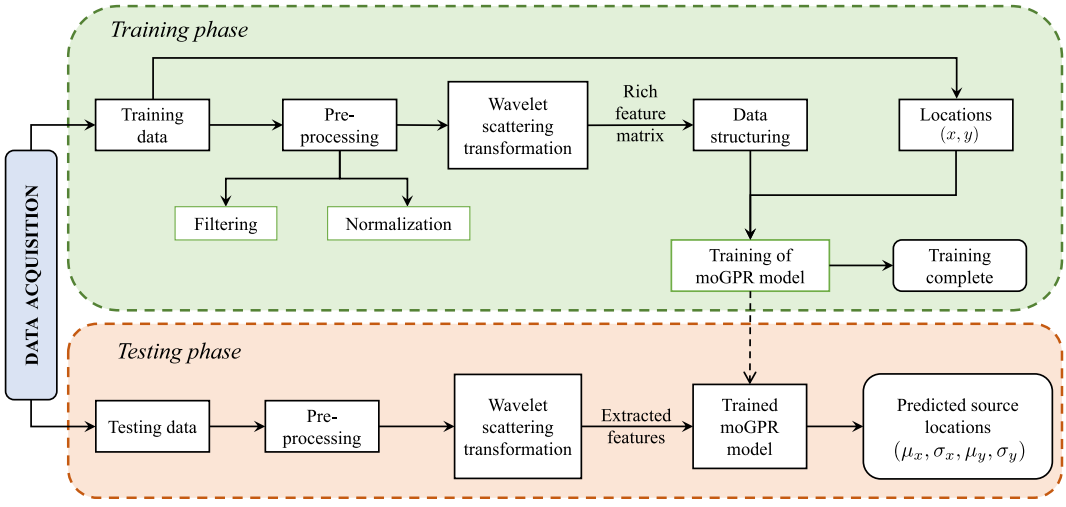

Fig. 3. Flow chart illustrating the complete algorithm for probabilistic estimation of acoustic source location.

Step 2 - Feature extraction with wavelet scattering. Wavelet scattering transformation decomposes the normalized signal into zeroth order, first order, and second order frequency spectrum. This 3rd order decomposition provides a deeper understanding of signals. The 1st order focuses on the overall energy distribution, the 2nd order captures modulations within the signal, 3rd order captures higher-order interactions which potentially differentiate between closely spaced features in the signal. Thus, we obtain rich feature matrix which is mapped to the location of acoustic source through multi-output Gaussian process regression (moGPR).

Step 3 - Data structuring for moGPR. Once the training feature matrix is developed, the outputs as well as input feature matrix are reorganized to fit into a structured format of coregionalisation kernel in moGPR. The target variables are defined as the known source locations during the model training phase, facilitating the moGPR model's learning process.

Step 4 - moGPR model training. The structured data serves as the input training dataset to the moGPR model. This phase involves training the model on the extracted feature matrix and their corresponding source locations. Unlike traditional Gaussian process regression, moGPR is adept at handling multiple outputs that incorporates the correlations between impact locations. The hyperparameters are optimized through global optimization methods and model accuracy is evaluated on validation set.

Step 5 - Source localization using trained moGPR model. For new AE events, the algorithm extracts features using the same wavelet scattering process and inputs them into the trained moGPR model. The model then predicts the locations of the AE sources based on these features, leveraging its learned correlations and the robustness of the wavelet-transformed features.

This proposed method accurately localizes AE sources and has been compared with traditional approaches as discussed in the next section.

5. Results and discussion

The proposed framework, which integrates the wavelet scattering transform with multi-output Gaussian process regression (moGPR), was rigorously tested through an experimental study as previously described. To evaluate the effectiveness of this framework, the study compared it against several alternative approaches. These include combinations of time of flight (TOF) with artificial neural networks (ANN), TOF with Gaussian process regression (GPR), TOF with multi-output Gaussian process regression (moGPR), as well as the integration of wavelet scattering transform (WST) with ANN, WST with GPR, and WST with moGPR. The experimental results showcase the typical acoustic response captured by five sensors (S1 to S5) following the impact of a Teflon sphere on a CFRP (Carbon Fiber Reinforced Polymer) surface, as illustrated in Fig. 4 The authors have presented the results obtained from these approaches into two categories based on feature-extracting technique (A) Time of flight (TOF) of acoustic response and (B) Wavelet

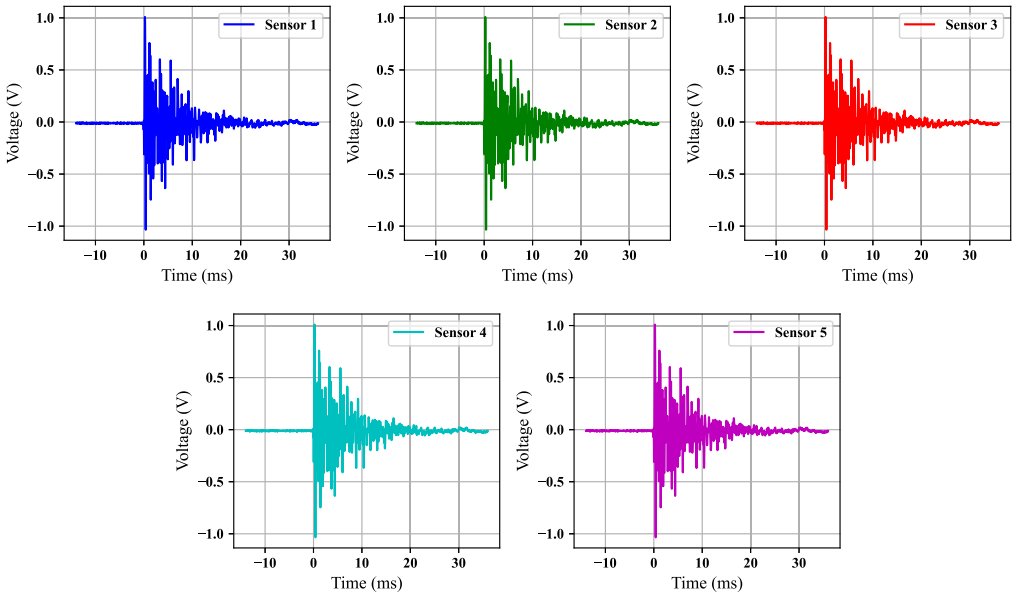

Fig. 4. The typical acoustic response obtained through five sensors when Teflon sphere provides impact to the CFRP composite.

scattering transform for extracting Lamb wave signatures. For feature extraction of the first category, the research uses a methodical approach for determining the signal's arrival time through the threshold crossing of its envelope. The process of calculating the envelope involves defining the analytic signal $x_A(t)$ for a given real signal $x(t)$, which is expressed as:

$$x_A(t) = x(t) + i \cdot x_H(t) \tag{18}$$

In this equation, i stands for the square root of -1, and $x_H(t)$ represents the Hilbert transform of $x(t)$, given by:

$$x_H(t) = \frac{1}{\pi} \int_{-\infty}^{\infty} x(\tau) \cdot \frac{1}{t-\tau} d\tau \tag{19}$$

Subsequently, the signal's envelope, $A(t)$, is derived using $A(t) = \sqrt{x(t)^2 + x_H(t)^2}$. The time of flight is accurately determined at the juncture where the signal's envelope exceeds a predetermined threshold level (A_t), which, in this paper, is set at 0.1 V. The intention of discussing the results from the time of flight approaches is to compare the proposed framework (WST + moGPR) with the traditional approaches of feature extraction.

A Teflon sphere is dropped on 82 different locations of the plate out of which acoustic response from the 72 locations are used for training the probabilistic machine learning models and the remaining 10 are used for testing and validating the model prediction accuracy. The collocation points described as training and testing points are illustrated in Fig. 5. The points marked with a star in red color are the testing points and the dots in blue color show the training points. The next subsections will discuss the result of impact localization for these two categories.

5.1. Impact localization using time of flight (TOF) of acoustic response

In this section, we have utilized the artificial neural network (ANN), Gaussian process regression (GPR), and multi-output Gaussian process regression for mapping the time of flight response to the source locations. ANN has the limitation that it does not account for uncertainties arises due to perturbations in the time of flight observations. The ANN model has five inputs comprised of time of flight information measured from 5 sensors installed on the CFRP plate. The network predicts two outputs corresponding to the x- and y- coordinates of the estimated locations inherently accounting the correlation between

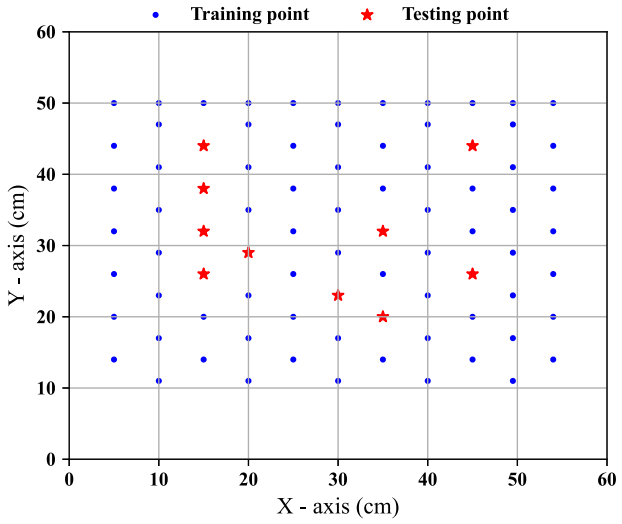

Fig. 5. Training and testing collocation points used for training and validation of the proposed probabilistic machine learning framework.

coordinates. The prediction made by the ANN model using time of flight observations is illustrated graphically in Fig. 6(a). Further, the next model used for comparison is Gaussian process regression which is probabilistic in nature, however, does not account the correlation among coordinates. The GPR uses a radial basis kernel function for the input–output mapping. The paper proposes the multi-output Gaussian process regression (moGPR) for accounting the correlation among coordinates and uncertainties in measurement. The prediction made by GPR and moGPR models is graphically illustrated in Fig. 6 (b,c). Moreover, the estimated values of X and Y ordinates with ANN, GPR, moGPR model and standard deviation obtained using GPR, moGPR model is provided in Table 2.

To evaluate the accuracy of the results, the absolute error in the respective direction and a displacement error function ϵ_r based on root-mean-square error is defined as $\epsilon_r = \sqrt{(\mu_x - x)^2 + (\mu_y - y)^2}$ where, (x, y) are the true impact coordinates and (μ_x, μ_y) are the estimated coordinates. Table 3 summarizes the absolute error and displacement

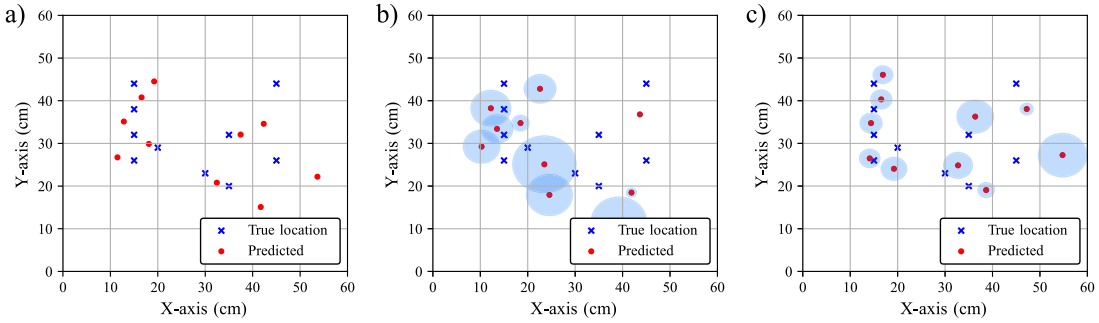

Fig. 6. True and estimated locations of the testing points using (a) TOF + ANN, (b) TOF + GPR, and (c) TOF + moGPR approaches. The bubble in sky blue color as shown in (b) and (c) are the standard deviation obtained using the probabilistic model.

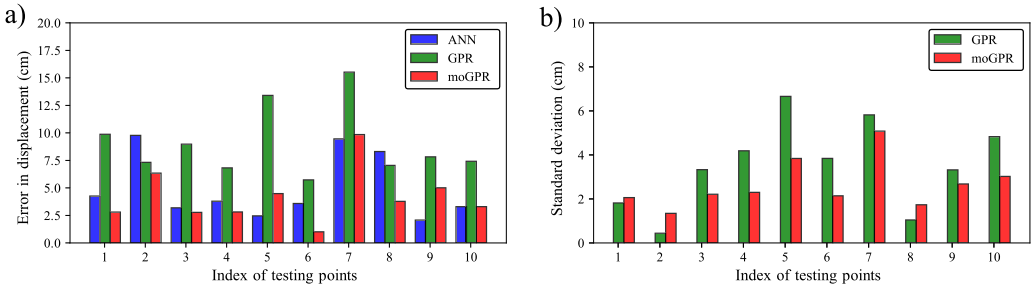

Fig. 7. This figure demonstrate (a) the net error ϵ_r, and (b) standard deviation obtained using TOF + ANN, TOF + GPR, and TOF + moGPR. It can be clearly seen that error obtained for the GPR case is large as it does not account the correlation in the output. Similarly, the standard deviation in case of GPR is high.

Table 2
True and estimated coordinates obtained using time of flight based frameworks.

True locations (cm)		Predicted locations (cm)							
		ANN		GPR			moGPR		
x	y	μ_x	μ_y	μ_x	μ_y	σ	μ_x	μ_y	σ
15	44	19.228	44.523	18.479	34.758	1.910	16.887	46.074	2.168
45	44	42.330	34.596	43.650	36.801	0.464	47.218	38.055	1.414
15	38	16.574	40.776	22.591	42.791	3.504	16.542	40.310	2.328
15	32	12.832	35.113	12.225	38.233	4.406	14.382	34.748	2.418
35	32	37.459	32.064	23.511	25.086	7.010	36.358	36.274	4.040
15	26	11.489	26.726	10.275	29.243	4.044	14.110	26.480	2.254
45	26	53.657	22.196	39.203	11.599	6.126	54.769	27.252	5.348
35	20	41.702	15.093	41.879	18.471	1.098	38.661	19.068	1.826
20	29	18.116	29.877	13.528	33.398	3.494	19.217	24.049	2.280
30	23	32.442	20.788	24.577	17.934	5.084	32.730	24.849	3.180

error obtained in estimating the location of impact using data-driven ANN, GPR, moGPR. It is observed from Table 3 that the performance of the data-driven ANN, GPR with time of flight observations in the prediction of AE source location is very poor in comparison of TOF plus moGPR combination with an average error of 5.0202, 8.9955, 4.2178 cm. This clearly indicates the results of moGPR shows improvement relative of ANN and GPR results. Further, the error chart and difference in standard deviation are provided in Fig. 7. It shows that the error obtained in the case of GPR is enormous as it cannot account for the output correlation.

Table 3
Absolute and net error obtained using time of flight based frameworks for testing points.

ANN			GPR			moGPR		
ϵ_x	ϵ_y	ϵ_r	ϵ_x	ϵ_y	ϵ_r	ϵ_x	ϵ_y	ϵ_r
4.228	0.523	4.260	3.479	9.241	9.875	1.887	2.074	2.804
2.669	9.403	9.775	1.350	7.198	7.324	2.218	5.944	6.345
1.574	2.776	3.191	7.591	4.791	8.977	1.542	2.310	2.777
2.167	3.113	3.793	2.774	6.233	6.822	0.617	2.748	2.816
2.459	0.064	2.460	11.488	6.913	13.408	1.358	4.274	4.485
3.510	0.726	3.585	4.724	3.243	5.730	0.890	0.480	1.011
8.657	3.803	9.455	5.796	14.400	15.523	9.769	1.252	9.849
6.702	4.907	8.307	6.879	1.528	7.047	3.661	0.931	3.778
1.883	0.877	2.077	6.471	4.398	7.825	0.782	4.950	5.012
2.442	2.212	3.295	5.422	5.065	7.420	2.730	1.849	3.298

5.2. Impact localization using Lamb wave signature directly through WST

In this section, we have utilized the artificial neural network (ANN), Gaussian process regression (GPR), and multi-output Gaussian process regression for mapping the Lamb wave signature represented by feature matrix of wavelet scattering transform to the source locations. The typical results obtained for the second-order WST is illustrated in Fig. 8

The feature matrix is developed using WST which is flattened before submitting it to machine learning models. The ANN model has input whose size is compatible with the flattened array that comprises WST rich feature matrix. The network predicts two outputs corresponding to the x- and y-coordinates of the estimated locations inherently accounting for the correlation between coordinates. The prediction made by the ANN model using time of flight observations is illustrated graphically in Fig. 9(a). Further, the next model used for comparison is Gaussian process regression which is probabilistic in nature, however, does not

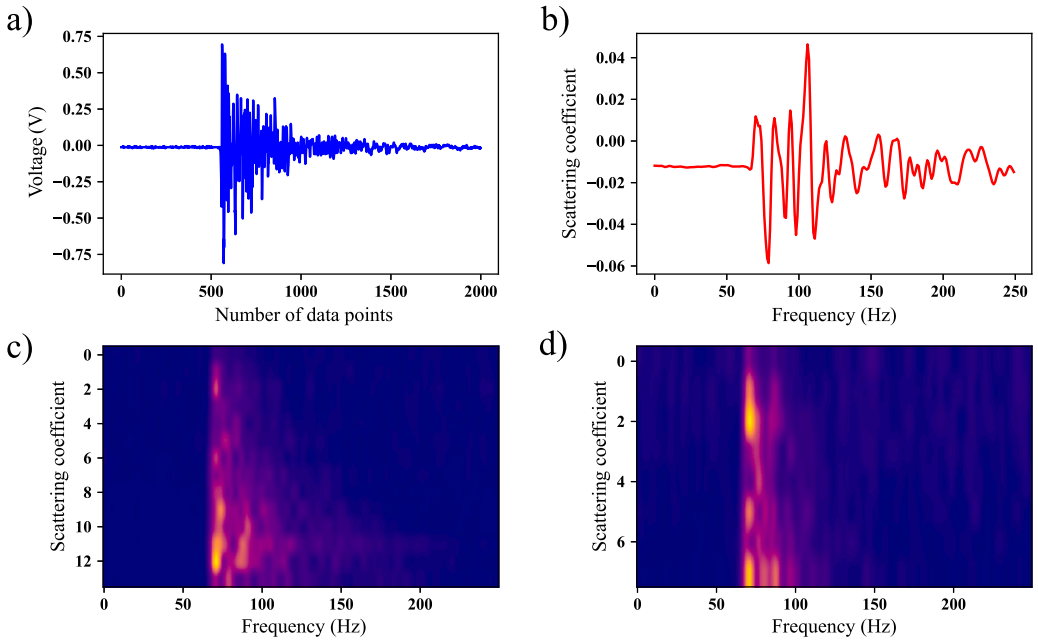

Fig. 8. The decomposition of signal through wavelet scattering transform (a) original acoustic response, (b) zeroth order coefficients, (c) first-order coefficients, and (d) second-order coefficients. This decomposition represents the Lamb wave signatures which is mapped to the source locations using probabilistic machine learning frameworks.

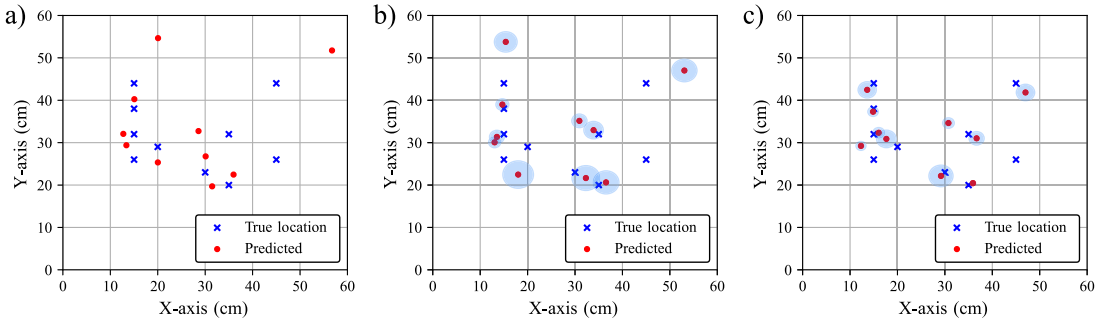

Fig. 9. True and estimated locations of the testing points using (a) WST + ANN, (b) WST + GPR, and (c) WST + moGPR approaches. The bubbles in sky blue color as shown in (b) and (c) are the standard deviation obtained using the probabilistic model.

Table 4
True and estimated coordinates obtained using wavelet scattering-based frameworks.

True		Predicted locations (cm)							
locations (cm)		ANN		GPR			moGPR		
x	y	μ_x	μ_y	μ_x	μ_y	σ	μ_x	μ_y	σ
15	44	20.060	54.652	15.390	53.768	2.520	13.616	42.460	2.016
45	44	56.751	51.745	53.063	47.016	2.790	47.001	41.838	2.034
15	38	15.060	40.250	14.675	38.985	1.430	14.857	37.297	1.162
15	32	12.736	32.073	13.524	31.352	1.635	16.046	32.329	1.294
35	32	28.594	32.730	30.917	35.143	1.680	30.754	34.625	1.292
15	26	13.386	29.387	13.041	30.077	1.325	12.304	29.230	1.100
45	26	30.100	26.762	33.912	32.954	2.150	36.693	31.023	1.668
35	20	35.985	22.467	36.537	20.630	2.855	35.921	20.445	0.580
20	29	20.019	25.335	18.007	22.470	3.390	17.660	30.882	2.166
30	23	31.472	19.699	32.292	21.651	3.075	29.176	22.150	2.670

account for the correlation amount coordinates. The GPR uses a radial basis kernel function for the input–output mapping. The paper proposes a novel framework that constitutes the wavelet scattering transform (WST) with multi-output Gaussian process regression (moGPR) for accounting the correlation among coordinates and uncertainties in measurement. The prediction made by GPR and moGPR models is graphically illustrated in Fig. 9 (b,c). Moreover, the estimated values of X and Y ordinates with ANN, GPR, moGPR model and standard deviation obtained using GPR, moGPR model is provided in Table 4.

The accuracy of the results is evaluated in the same fashion as discussed in the previous section. Table 5 summarizes the absolute error and displacement error obtained in estimating the location of impact using data-driven ANN, GPR, moGPR. It is observed from Table 5 that the performance of the data-driven ANN, GPR with time of flight observations in the prediction of AE source location is very poor in

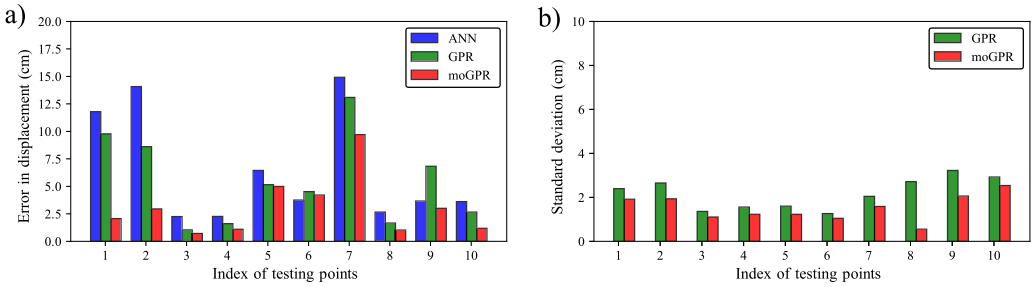

Fig. 10. This figure demonstrate (a) the net error ϵ_r, and (b) standard deviation obtained using WST + ANN, WST + GPR, and WST + moGPR. It can be clearly seen that the proposed approach WST + moGPR has the minimum error relative to other approaches as well as the standard deviation obtained are within practical limits.

Table 5
Absolute and net error obtained using wavelet scattering transform-based frameworks for testing points.

ANN			GPR			moGPR		
ϵ_x	ϵ_y	ϵ_r	ϵ_x	ϵ_y	ϵ_r	ϵ_x	ϵ_y	ϵ_r
5.060	10.652	11.793	0.390	9.768	9.776	1.383	1.539	2.069
11.751	7.745	14.074	8.063	3.016	8.609	2.001	2.161	2.946
0.060	2.250	2.251	0.324	0.985	1.037	0.143	0.702	0.716
2.263	0.073	2.265	1.475	0.647	1.611	1.046	0.329	1.097
6.405	0.730	6.447	4.082	3.143	5.152	4.245	2.625	4.991
1.613	3.387	3.752	1.958	4.077	4.522	2.695	3.230	4.207
14.899	0.762	14.919	11.087	6.954	13.088	8.306	5.023	9.707
0.985	2.467	2.657	1.537	0.630	1.661	0.921	0.445	1.022
0.019	3.664	3.664	1.992	6.529	6.826	2.339	1.882	3.003
1.472	3.300	3.614	2.292	1.348	2.659	0.823	0.849	1.183

Table 6
The final comparison of average and maximum error obtained while estimating source locations using different approaches.

Framework	Average error (cm)	Maximum error (cm)
TOF + ANN	5.020	9.775
TOF + GPR	8.995	15.523
TOF + moGPR	4.217	9.849
WST + ANN	6.543	14.919
WST + GPR	5.494	13.088
WST + moGPR	**3.094**	**9.707**

comparison of WST plus moGPR combination with an average error of 6.543, 5.494, 3.094 cm. This clearly indicates the results of moGPR are far superior relative of ANN and GPR results. Further, the error chart and the difference in standard deviation obtained for WST frameworks are provided in Fig. 10.

5.3. Comparison of results of impact localization using TOF and Lamb wave signatures directly

The results obtained from WST + moGPR are found to the most accurate among all the proposed approaches as shown in Table 6. It summarizes the average error and maximum error obtained in the estimation through six approaches. The results obtained using the proposed probabilistic framework are considerably more accurate as compared to other data-driven ANN and time of flight-based methods with an average error of 3.094 cm.

6. Conclusion

This study presents a probabilistic approach to acoustic emission (AE) source localization by integrating wavelet scattering transformation (WST) for feature extraction with multi-output Gaussian Process Regression (moGPR). WST effectively extracts informative features from the captured Lamb waves, while moGPR models the correlated spatial coordinates of the impact location and accounts for uncertainties within the data. By integrating wavelet scattering transform (WST) for feature extraction, the framework captures the nuanced details embedded within Lamb wave signatures, unlike traditional methods that often rely on simplistic time-of-flight or basic statistical features. This enhanced feature representation allows for a more accurate and comprehensive understanding of the wave propagation phenomenon, especially in complex anisotropic materials where directional wave velocity variations challenge conventional techniques. In addition to superior feature extraction, the framework's incorporation of multi-output Gaussian Process Regression (moGPR) which is a probabilistic model that not only provides precise source localization but also quantifies uncertainties, offering valuable confidence intervals for decision-making. The experimental validation using a CFRP composite panel equipped with a sparse sensor array confirmed the effectiveness of the proposed method. The results show that the proposed approach (WST + moGPR) can accurately estimate AE source locations with an average error of 3.094 cm, as compared to the other approaches based on time of flight observations which has an average error ranging from 5 cm to 10 cm. The incorporation of Lamb wave signatures as input features results in a consistent accuracy improvement across all three models (ANN, GPR, and moGPR), suggesting a strong correlation between these features and accurate AE source localization. The results further demonstrate that the framework successfully addresses measurement uncertainties, leading to reliable impact source localization with confidence intervals rather than the point-estimate, and output correlation which is neglected in the case of GPR. Thus, by explicitly modeling the inherent correlation between impact location coordinates, moGPR outperforms methods that treat coordinates independently, resulting in more consistent and reliable localization. Next, the framework does not require the vast amounts of training data often demanded by deep learning approaches. This makes it a viable option for real-world scenarios where data collection is limited or expensive.

Future research could explore the framework's applicability to diverse materials and complex geometries. Additionally, evaluating the method's robustness under varying noise levels, disturbances (*e.g.*, vibrations, temperature fluctuations), and sensor configurations can be analyzed. This includes analyzing sensitivity, outlier handling, and exploring strategies like incorporating physics-informed priors to moGPR

or advanced denoising techniques. Further, integrating time-of-flight equations into the Bayesian machine learning framework can improve localization accuracy. Additionally, investigating advanced algorithms like Bayesian neural networks and physics-informed Bayesian neural networks could offer more robust and accurate solutions for acoustic source localization.

Overall, the proposed algorithm marks a significant step forward for AE source localization. It showcases the power of combining advanced signal processing with machine learning to address complex engineering challenges. This research offers valuable insights into the future of SHM, contributing to safer and more reliable monitoring of critical infrastructure.

Funding

The authors would like to acknowledge Indian Space Research Organization (ISRO) for supporting this work under grant number ISRO/RES/STC/IITG/2021-22.

CRediT authorship contribution statement

Shivam Ojha: Writing – review & editing, Writing – original draft, Validation, Methodology, Formal analysis. **Naveen Jangid:** Data curation, Formal analysis, Writing – review & editing. **Amit Shelke:** Writing – review & editing, Validation, Supervision, Resources, Conceptualization. **Anowarul Habib:** Writing – review & editing, Validation, Supervision, Investigation, Funding acquisition, Data curation, Conceptualization.

Declaration of competing interest

The authors have no conflicts of interest that are relevant to the content of this article.

Data availability

Data will be made available on request.

References

[1] W. Staszewski, C. Boller, G.R. Tomlinson, Health Monitoring of Aerospace Structures: Smart Sensor Technologies and Signal Processing, John Wiley & Sons, 2004.
[2] P. Coverley, W. Staszewski, Impact damage location in composite structures using optimized sensor triangulation procedure, Smart Mater. Struct. 12 (5) (2003) 795.
[3] K.V. Jata, T. Kundu, T.A. Parthasarathy, An introduction to failure mechanisms and ultrasonic inspection, in: Advanced Ultrasonic Methods for Material and Structure Inspection, Wiley Online Library, 2007, pp. 1–42.
[4] V. Giurgiutiu, Lamb wave generation with piezoelectric wafer active sensors for structural health monitoring, in: Smart Structures and Materials 2003: Smart Structures and Integrated Systems, vol. 5056, SPIE, 2003, pp. 111–122.
[5] A.K. Mal, F. Shih, S. Banerjee, Acoustic emission waveforms in composite laminates under low velocity impact, in: Smart Nondestructive Evaluation and Health Monitoring of Structural and Biological Systems II, vol. 5047, SPIE, 2003, pp. 1–12.
[6] A.K. Mal, F. Ricci, S. Gibson, S. Banerjee, Damage detection in structures from vibration and wave propagation data, in: Smart Nondestructive Evaluation and Health Monitoring of Structural and Biological Systems II, vol. 5047, SPIE, 2003, pp. 202–210.
[7] A. Kahirdeh, M. Naderi, M. Khonsari, On the role of cooling on fatigue failure of a woven glass/epoxy laminate, J. Compos. Mater. 47 (15) (2013) 1803–1815.
[8] A. Bagheri, K. Li, P. Rizzo, Reference-free damage detection by means of wavelet transform and empirical mode decomposition applied to lamb waves, J. Intell. Mater. Syst. Struct. 24 (2) (2013) 194–208.
[9] A. Farhidzadeh, E. Dehghan-Niri, S. Salamone, B. Luna, A. Whittaker, Monitoring crack propagation in reinforced concrete shear walls by acoustic emission, J. Struct. Eng. 139 (12) (2013) 04013010.
[10] L. Gaul, S. Hurlebaus, Identification of the impact location on a plate using wavelets, Mech. Syst. Signal Process. 12 (6) (1998) 783–795.
[11] M. Meo, G. Zumpano, M. Piggott, G. Marengo, Impact identification on a sandwich plate from wave propagation responses, Compos. Struct. 71 (3–4) (2005) 302–306.
[12] F. Ciampa, M. Meo, A new algorithm for acoustic emission localization and flexural group velocity determination in anisotropic structures, Composites A 41 (12) (2010) 1777–1786.
[13] T. Kundu, S. Das, K.V. Jata, Point of impact prediction in isotropic and anisotropic plates from the acoustic emission data, J. Acoust. Soc. Am. 122 (4) (2007) 2057–2066.
[14] T. Kundu, S. Das, K.V. Jata, Detection of the point of impact on a stiffened plate by the acoustic emission technique, Smart Mater. Struct. 18 (3) (2009) 035006.
[15] T. Hajzargerbashi, T. Kundu, S. Bland, An improved algorithm for detecting point of impact in anisotropic inhomogeneous plates, Ultrasonics 51 (3) (2011) 317–324.
[16] C. Yang, Z. Fan, Y. Xia, Convex model-based reduced-order model for uncertain control systems, IEEE Trans. Syst., Man, Cybern.: Syst. (2024).
[17] C. Yang, W. Lu, Y. Xia, Positioning accuracy analysis of industrial robots based on non-probabilistic time-dependent reliability, IEEE Trans. Reliab. (2023).
[18] C. Yang, H. Ouyang, A novel load-dependent sensor placement method for model updating based on time-dependent reliability optimization considering multi-source uncertainties, Mech. Syst. Signal Process. 165 (2022) 108386.
[19] S. Ojha, N.M. Kalimullah, A. Shelke, Application of constrained unscented Kalman filter (CUKF) for system identification of coupled hysteresis under bidirectional excitation, Struct. Control Health Monit. 29 (12) (2022) e3115.
[20] C. Yang, W. Lu, Y. Xia, Reliability-constrained optimal attitude-vibration control for rigid-flexible coupling satellite using interval dimension-wise analysis, Reliab. Eng. Syst. Saf. 237 (2023) 109382.
[21] C. Yang, Interval strategy-based regularization approach for force reconstruction with multi-source uncertainties, Comput. Methods Appl. Mech. Engrg. 419 (2024) 116679.
[22] E.D. Niri, A. Farhidzadeh, S. Salamone, Nonlinear Kalman filtering for acoustic emission source localization in anisotropic panels, Ultrasonics 54 (2) (2014) 486–501.
[23] E.D. Niri, S. Salamone, A probabilistic framework for acoustic emission source localization in plate-like structures, Smart Mater. Struct. 21 (3) (2012) 035009.
[24] E. Dehghan Niri, A. Farhidzadeh, S. Salamone, Adaptive multisensor data fusion for acoustic emission source localization in noisy environment, Struct. Health Monit. 12 (1) (2013) 59–77.
[25] A. Mostafapour, S. Davoodi, M. Ghareaghaji, Acoustic emission source location in plates using wavelet analysis and cross time frequency spectrum, Ultrasonics 54 (8) (2014) 2055–2062.
[26] M. Koabaz, T. Hajzargarbashi, T. Kundu, M. Deschamps, Locating the acoustic source in an anisotropic plate, Struct. Health Monit. 11 (3) (2012) 315–323.
[27] A. Ebrahimkhanlou, S. Salamone, Acoustic emission source localization in thin metallic plates: A single-sensor approach based on multimodal edge reflections, Ultrasonics 78 (2017) 134–145.
[28] T. Kundu, X. Yang, H. Nakatani, N. Takeda, A two-step hybrid technique for accurately localizing acoustic source in anisotropic structures without knowing their material properties, Ultrasonics 56 (2015) 271–278.
[29] J. Tai, T. He, Q. Pan, D. Zhang, X. Wang, A fast beamforming method to localize an acoustic emission source under unknown wave speed, Materials 12 (5) (2019) 735.
[30] S. Ojha, A. Shelke, S.B. Tiwari, B. Santhosh, S. Thomas, A. Habib, Damage localization in plates using energy of acoustic emission through Gaussian process regression, in: 50th Annual Review of Progress in Quantitative Nondestructive Evaluation, vol. 87202, American Society of Mechanical Engineers, 2023, V001T09A006.
[31] N.M.-M. Kalimullah, A. Shelke, A. Habib, A probabilistic framework for source localization in anisotropic composite using transfer learning based multi-fidelity physics informed neural network (mfPINN), Mech. Syst. Signal Process. 197 (2023) 110360.
[32] B.A. Zárate, A. Pollock, S. Momeni, O. Ley, Structural health monitoring of liquid-filled tanks: A Bayesian approach for location of acoustic emission sources, Smart Mater. Struct. 24 (1) (2014) 015017.
[33] M.S. Hameed, Z. Li, J. Chen, J. Qi, Lamb-wave-based multistage damage detection method using an active PZT sensor network for large structures, Sensors 19 (9) (2019) 2010.
[34] S.K. Al-Jumaili, M.R. Pearson, K.M. Holford, M.J. Eaton, R. Pullin, Acoustic emission source location in complex structures using full automatic delta t mapping technique, Mech. Syst. Signal Process. 72 (2016) 513–524.
[35] M.R. Pearson, M. Eaton, C. Featherston, R. Pullin, K. Holford, Improved acoustic emission source location during fatigue and impact events in metallic and composite structures, Struct. Health Monit. 16 (4) (2017) 382–399.
[36] D. Li, J.-H. Nie, W.-X. Ren, W.-H. Ng, G.-H. Wang, Y. Wang, A novel acoustic emission source location method for crack monitoring of orthotropic steel plates, Eng. Struct. 253 (2022) 113717.
[37] L. Cheng, H. Xin, R.M. Groves, M. Veljkovic, Acoustic emission source location using lamb wave propagation simulation and artificial neural network for I-shaped steel girder, Constr. Build. Mater. 273 (2021) 121706.

[38] A. Jierula, S. Wang, T.-M. Oh, J.-W. Lee, J.H. Lee, Detection of source locations in RC columns using machine learning with acoustic emission data, Eng. Struct. 246 (2021) 112992.
[39] J. Hensman, R. Mills, S. Pierce, K. Worden, M. Eaton, Locating acoustic emission sources in complex structures using Gaussian processes, Mech. Syst. Signal Process. 24 (1) (2010) 211–223.
[40] M.R. Jones, T.J. Rogers, K. Worden, E.J. Cross, A Bayesian methodology for localising acoustic emission sources in complex structures, Mech. Syst. Signal Process. 163 (2022) 108143.
[41] M. Jones, T. Rogers, K. Worden, E. Cross, Heteroscedastic Gaussian processes for localising acoustic emission, in: Data Science in Engineering, Volume 9: Proceedings of the 39th IMAC, a Conference and Exposition on Structural Dynamics 2021, Springer, 2022, pp. 185–197.
[42] S. Mallat, Group invariant scattering, Comm. Pure Appl. Math. 65 (10) (2012) 1331–1398.
[43] J. Bruna, S. Mallat, Invariant scattering convolution networks, IEEE Trans. Pattern Anal. Mach. Intell. 35 (8) (2013) 1872–1886.
[44] S. Mallat, Understanding deep convolutional networks, Phil. Trans. R. Soc. A 374 (2065) (2016) 20150203.
[45] A.W. Amer, S. Roy, F. Kopsaftopoulos, Probabilistic SHM under varying loads via the integration of Gaussian process regression and physics-based guided-wave propagation models, in: AIAA Scitech 2021 Forum, 2021, p. 0434.
[46] Q.-A. Wang, C. Zhang, Z.-G. Ma, Y.-Q. Ni, Modelling and forecasting of SHM strain measurement for a large-scale suspension bridge during typhoon events using variational heteroscedastic Gaussian process, Eng. Struct. 251 (2022) 113554.
[47] H. Liu, J. Cai, Y.-S. Ong, Remarks on multi-output Gaussian process regression, Knowl.-Based Syst. 144 (2018) 102–121.
[48] R. Leonarduzzi, H. Liu, Y. Wang, Scattering transform and sparse linear classifiers for art authentication, Signal Process. 150 (2018) 11–19.
[49] J. Bruna, S. Mallat, Classification with scattering operators, in: CVPR 2011, IEEE, 2011, pp. 1561–1566.
[50] J. Andén, S. Mallat, Deep scattering spectrum, IEEE Trans. Signal Process. 62 (16) (2014) 4114–4128.
[51] J. Andén, S. Mallat, Multiscale scattering for audio classification., in: ISMIR, Miami, Florida, 2011, pp. 657–662.
[52] C. Rasmussen, C. Williams, Gaussian Processes for Machine Learning, MIT Press, Cambridge, MA, 2006.
[53] M. Van der Wilk, V. Dutordoir, S. John, A. Artemev, V. Adam, J. Hensman, A framework for interdomain and multioutput Gaussian processes, 2020, arXiv preprint arXiv:2003.01115.
[54] M.A. Alvarez, L. Rosasco, N.D. Lawrence, et al., Kernels for vector-valued functions: A review, Found. Trends® Mach. Learn. 4 (3) (2012) 195–266.
[55] C.A. Micchelli, M. Pontil, On learning vector-valued functions, Neural Computation 17 (1) (2005) 177–204.
[56] H. Kadri, E. Duflos, P. Preux, S. Canu, A. Rakotomamonjy, J. Audiffren, Operator-valued kernels for learning from functional response data, J. Mach. Learn. Res. 17 (20) (2016) 1–54.
[57] E.V. Bonilla, K. Chai, C. Williams, Multi-task Gaussian process prediction, in: Advances in Neural Information Processing Systems, vol. 20, 2007.